Inorg. Chem. **2002**, *41*, 4633–4641

A Periodic Walk: A Series of First-Row Transition Metal Complexes with the Pentadentate Ligand PY5†

Robertus J. M. Klein Gebbink, Robert T. Jonas, Christian R. Goldsmith, and T. Daniel P. Stack*

Department of Chemistry, Stanford University, California 94305

Received March 26, 2002

A series of transition metal complexes derived from the pentadentate ligand PY5, 2,6-(bis-(bis-2-pyridyl)-methoxymethane)pyridine, illustrates the intrinsic propensity of this ligand to complex metal ions. X-ray structural data are provided for six complexes (**1**–**6**) with cations of the general formula $[M^{II}(PY5)(Cl)]^+$, where M = Mn, Fe, Co, Ni, Cu, Zn. In complexes **1**–**4** and **6**, the metal ions are coordinated in a distorted-octahedral fashion; the four terminal pyridines of PY5 occupy the equatorial sites while the axial positions are occupied by the bridging pyridine of PY5 and a chloride anion. Major distortions from an ideal octahedral geometry arise from displacement of the metal atom from the equatorial plane toward the chloride ligand and from differences in pyridine–metal–pyridine bond angles. The series of complexes shows that M(II) ions are consistently accommodated in the ligand by displacement of the metal ion from the PY5 pocket, a tilting of the axial pyridine subunit, and nonsymmetrical pyridine subunit ligation in the equatorial plane. The displacement from the ligand pocket increases with the ionic radius of M(II). The axial pyridine tilt, however, is approximately the same for all complexes and appears to be independent of the electronic ground state of M(II). In complex **5**, the Cu(II) ion is coordinated by only four of the five pyridine subunits of the ligand, resulting in a square-pyramidal complex. The overall structural similarity of **5** with the other complexes reflects the strong tendency of PY5 to enforce a distorted-octahedral coordination geometry. Complexes **1**–**6** are further characterized in terms of solution magnetic susceptibility, electrochemical behavior, and optical properties. These show the high-spin nature of the complexes and the anticipated stabilization of the divalent oxidation state.

Introduction

Modeling of the transition metal ligation motifs found in metalloenzymes and studying the chemistry of intermediate species derived from model compounds are two important areas of research within the field of bioinorganic chemistry.[1] A promising strategy is the development of well-defined coordination geometries for monomeric metal sites that do not significantly alter upon oxidation or substrate binding. Ligands that impose a particular coordination geometry can reduce the complexity of reactivity studies of metal complexes in homogeneous solutions, potentially leading to the characterization of reactive intermediates. Examples of this ligand-enforced-geometry approach include the study of metalloporphyrin complexes as models for heme-containing proteins.[2] Similar examples are also found in non-heme Cu- and Fe-dioxygen chemistry[3−7] and in Fe_4S_4 chemistry.[8,9]

Our interest in mononuclear first-row transition metal centers possessing a single labile coordination site was initially motivated by lipoxygenase, a mononuclear iron enzyme involved in fatty acid metabolism.[10,11] While numerous pentadentate oligoamine ligands, such as derivatized

* To whom correspondence should be addressed. E-mail: stack@stanford.edu. Phone: (650) 725-8736. Fax: (650) 725-0259.

† Dedicated to Professor K. Weighardt on the occasion of his 60th birthday.

(1) Lippard, S. J.; Berg, J. M. *Principles of Bioinorganic Chemistry*; University Science Books: Mill Valley, CA, 1994.
(2) Momenteau, M.; Reed, C. A. *Chem. Rev.* **1994**, *94*, 659−698.
(3) Kitajima, N.; Moro-oka, Y. *Chem. Rev.* **1994**, *94*, 737−757.
(4) Que, L., Jr. *J. Chem. Soc., Dalton Trans.* **1997**, 3933−3940.
(5) Koch, W. O.; Kruger, H. J. *Angew. Chem., Int. Ed. Engl.* **1995**, *34*, 2671−2674.
(6) Schindler, S. *Eur. J. Inorg. Chem.* **2000**, *11*, 2311−2326.
(7) Du Bois, J.; Mizoguchi, T. J.; Lippard, S. J. *Coord. Chem. Rev.* **2000**, *200*, 443−485.
(8) Stack, T. D. P.; Holm, R. H. *J. Am. Chem. Soc.* **1988**, *110*, 2484−2494.
(9) Holm, R. H.; Ciurli, S.; Weigel, J. A. *Prog. Inorg. Chem.* **1990**, *38*, 1−74.
(10) Nelson, M. J.; Seitz, S. In *Active Oxygen in Biochemistry*; Valentine, J. S., Foote, C. S., Greenberg, A., Liebman, J. F., Eds.; Chapman and Hall: Glasgow, U.K., 1995; p 276−312.

10.1021/ic025617r CCC: $22.00
Published on Web 07/30/2002

Scheme 1

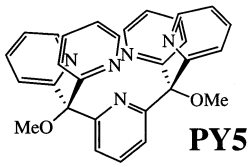

1 = [Mn(**PY5**)Cl]$_2$(MnCl$_4$)
2 = [Fe(**PY5**)Cl](Cl)
3 = [Co(**PY5**)Cl](Cl)
4 = [Ni(**PY5**)Cl](Cl)
5 = [Cu(**PY5**)Cl](Cl)
6 = [Zn(**PY5**)Cl]$_2$(ZnCl$_4$)

cyclams (1,4,8,11-tetraaza-cyclotetradecanes), are known to generate octahedral metal complexes via inclusion of an exogenous ligand, the number of noncyclic, pentadentate nitrogen ligands that impose an octahedral geometry to a transition metal is limited. Current examples involve a mixed monopyridine−tetra-amine ligand,[12] a structurally related monoamine−tetraimidazole ligand,[13] and a monoamine−tetrapyridine ligand.[14,15] Several open chain oligoamines are also known to function in a similar manner, including bleomycin analogues.[16] We report here a study on the coordination behavior of the ligand PY5, 2,6-(bis-(bis-2-pyridyl)methoxymethane)pyridine, that is predisposed to form a square-pyramidal, nitrogen coordination sphere for metals (Scheme 1, Figure 1). In earlier reports, we presented the lipoxygenase-like reactivity of [Fe^{III}(PY5)(OMe)]$^{2+}$,[17,18] and more recently, we have completed a study on a series of Fe(II) complexes, [Fe^{II}(PY5)(X)]$^{n+}$, that analyzed the effect of the exogenous ligand, X, on spectroscopic and structural properties.[19] This complementary study is aimed toward understanding the flexibility of the PY5 ligand to accommodate metal ions of various sizes. For that reason, a series of M(II) complexes (M = Mn, Fe, Co, Ni, Cu, Zn) with identical ligands has been synthesized and studied. At first glance, PY5 appears as a semirigid ligand with limited flexibility. However, subtle angular and torsional variations within the ligand framework allow it to accommodate variously sized M(II) ions of the first transition series.

Results

Synthesis. The numbering used for all the compounds discussed in this paper is shown in Scheme 1. Compounds

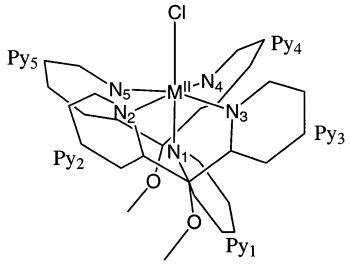

Figure 1. Schematic presentation of the octahedral metal(II) complexes formed by the PY5 ligand (double bonds are omitted for clarity). Py$_1$ is defined as the axial pyridine, and N$_{2-5}$ create the equatorial plane, Pl$_{eq}$.

1−**6** were synthesized by mixing equimolar amounts of the ligand PY5 and the appropriate divalent metal chloride salt in dry MeOH (eq 1). The yields of the recrystallized products ranged from 10% to 95%. All complexes are stable to O_2 and moisture.

$$MCl_2 + PY5 \rightarrow [M(PY5)Cl]^+ + Cl^- \quad (1)$$

$$3MCl_2 + 2PY5 \rightarrow 2[M(PY5)(Cl)]^+ + [MCl_4]^{2-} \quad (2)$$

The structures of the Mn and Zn products showed that the counteranions [Mn^{II}Cl$_4$]$^{2-}$ and [Zn^{II}Cl$_4$]$^{2-}$ formed during the preparation of **1** and **6**, respectively. These counterions cocrystallize with the [M^{II}(PY5)(Cl)]$^+$ cations in a 1:2 ratio ([M^{II}Cl$_4$]$^{2-}$/[M^{II}(PY5)(Cl)]$^+$). A 3:2 M^{II}Cl$_2$/PY5 ratio (eq 2) resulted in a higher yield for compound **1** (∼85%) but not for **6** (∼10%). A significantly higher yield (∼65%) of the [Zn^{II}(PY5)(Cl)]$^+$ cation could be obtained as the $CF_3SO_3^-$ salt, [Zn^{II}(PY5)(Cl)](CF_3SO_3), and this material is more synthetically tractable.

X-ray Structures: General Description. Single crystals of X-ray quality were obtained for all complexes in this series. For compounds **1**−**5**, this was achieved by means of vapor diffusion of Et_2O into a concentrated MeOH solution, whereas compound **6** crystallizes from an MeCN/H_2O solution after addition of Et_2O. Crystal data and data collection details are presented in Table 1. Selected bond lengths and angles for **1**−**6** are shown in Tables 2 and 3. The atom labeling scheme for the [M(PY5)(Cl)]$^{1+}$ cation is congruent for the six structures shown in Figures 2−4. In the case of **1**, two independent [Mn(PY5)(Cl)]$^{1+}$ cations exist in the asymmetric unit. For the purposes of the tables and metrical comparisons in this paper, the independent cations will be designated as **1(A)** and **1(B)**. While the crystallographic labeling scheme of the **1(A)** cation is congruent to the cation in **2**−**6**, that of **1(B)** is not. To facilitate structural comparisons, a congruent labeling scheme will be assumed for the **1(B)** cation.

In **1**−**4**, and **6**, the divalent metal ion is ligated in nearly identical six-coordinate geometries (Figures 2 and 3) by the five pyridine subunits of PY5 and an exogenous chloride anion. A singly charged cation results. The least-squares plane of the four nitrogen atoms of the terminal pyridines (N$_{2-5}$) conveniently defines an equatorial plane (Pl$_{eq}$), and the axial positions are occupied by the axial pyridine nitrogen (N$_1$) and the exogenous chloride. The metal ion is displaced from Pl$_{eq}$ toward the chloride in all structures; the displace-

(11) Samuelsson, B.; Dahlén, S.-E.; Lindgren, J. A.; Rouzer, C. A.; Serhan, C. N. *Science* **1987**, *237*, 1171−1176.
(12) Grohmann, A.; Knoch, F. *Inorg. Chem.* **1996**, *35*, 7932−7934.
(13) Tamagaki, S.; Kanamaru, Y.; Ueno, M.; Tagaki, W. *Bull. Chem. Soc. Jpn.* **1991**, *64*, 165−174.
(14) Lubben, M.; Meetsma, A.; Wilkinson, E. C.; Feringa, B. L.; Que, L., Jr. *Angew. Chem., Int. Ed. Engl.* **1995**, *34*, 1512−1514.
(15) Que, L., Jr.; Roelfes, G.; Lubben, M.; Chen, K.; Ho, R. Y. N.; Meetsma, A.; Genseberger, S.; Hermant, R. M.; Hage, R.; Mandal, S. K.; Young, V. G., Jr.; Zang, Y.; Kooijman, H.; Spek, A. L.; Feringa, B. L. *Inorg. Chem.* **1999**, *38*, 1929−1936.
(16) Nguyen, C.; Guajardo, R. J.; Mascharak, P. K. *Inorg. Chem.* **1996**, *35*, 6273−6281.
(17) Jonas, R. T.; Stack, T. D. P. *J. Am. Chem. Soc.* **1997**, *119*, 8566−8567.
(18) Goldsmith, C. R.; Jonas, R. T.; Stack, T. D. P. *J. Am. Chem. Soc.* **2002**, *124*, 83−96.
(19) See companion article: Goldsmith, C. R.; Jonas, R. T.; Cole, A. P.; Stack, T. D. P. *Inorg. Chem.* **2002**, *41*, 4642−4652.

Table 1. Crystal Data and Data Collection Details of **1**−**6**[a]

	1	**2**	**3**	**4**	**5**[b]	**6**[b]
formula	$C_{59}H_{54}N_{10}O_5Cl_6Mn_3$	$C_{31}H_{33}N_5O_4Cl_2Fe$	$C_{31}H_{33}N_5O_4Cl_2Co$	$C_{31}H_{33}N_5O_4Cl_2Ni$	$C_{29}H_{25}N_5O_2Cl_2Cu$	$C_{29}H_{27}N_5O_3Cl_3Zn_{1.5}$
fw	1360.67	666.39	651.46	669.24	610.00	697.99
machine type	CAD-4	CAD-4	CAD-4	CAD-4	Siemens Smart	Siemens Smart
temp (K)	203	203	203	203	161	175
space group	$P2_1/n$ (No. 14)	$P2_1/n$ (No. 14)	$P2_1/n$ (No. 14)	$P2_1/n$ (No. 14)	$C2/c$ (No. 15)	$P2_1/c$ (No. 14)
cryst syst	monoclinic	monoclinic	monoclinic	monoclinic	monoclinic	monoclinic
a (Å)	18.747(5)	12.807(2)	12.7975(2)	12.747(4)	23.5424(6)	10.7075(3)
b (Å)	14.555(4)	14.404(2)	14.4174(2)	14.389(7)	14.2882(4)	14.5730(2)
c (Å)	21.454(4)	16.550(2)	16.5256(3)	16.416(7)	19.7127(5)	18.7159(5)
β (deg)	93.936(2)	101.41(1)	100.994(1)	79.17(4)	112.664(1)	93.648(1)
V (Å^3)	5840(3)	2992.8(8)	2993.1(1)	2957(2)	6118.9(3)	2914.5(1)
Z	4	4	4	4	8	4
μ_{calcd} (cm^{-1})	9.70	7.28	7.93	8.83	9.2	15.6
F_{000}	2776.0	1384.00	1348.00	1392.00	2504.00	1424.00
d_{calcd} (g cm^{-3})	1.55	1.48	1.45	1.50	1.32	1.59
cryst size (mm^3)	0.50 × 0.40 × 0.40	0.45 × 0.30 × 0.20	0.50 × 0.40 × 0.20	0.60 × 0.60 × 0.20	0.26 × 0.23 × 0.15	0.17 × 0.13 × 0.03
p-factor	0.016	0.007	0.007	0.014	0.03	0.03
2θ range (deg)	4.42−50	4.58−50	4.26−50	5.66−50	3.24−52.20	2.79−52.20
no. reflns $I > 10\sigma(I)$	25	25	25	25	6792	4695
scan width	0.80 + 0.65 (tan θ)	0.76 + 0.66 (tan θ)	0.72 + 0.60 (tan θ)	1.56 + 1.10 (tan θ)	0.3°	0.3°
scan speed (ω, deg/min)	5.4	5.4	5.4	5.4	10-s frame exposure	20-s frame exposure
refls collected	11 004	5651	5732	10 810	14 676	13 817
unique reflns (R_{int})	10 701 (0.033)	5457 (0.038)	5476 (0.066)	7401 (0.063)	5640 (0.048)	5344 (0.08)
reflns with ($F_o^2 > 3\sigma(F_o^2)$)	6049	2650	3261	3595	3210	2547
no. variables	743	387	397	397	366	252
parameter-to-variable ratio	8.14	6.85	8.21	9.06	8.77	10.11
R (R_w)[c]	0.054 (0.057)	0.055 (0.049)	0.047 (0.048)	0.055 (0.050)	0.058 (0.076)	0.086 (0.098)
final diff ρ_{max}[d] (e$^-$/Å^3)	+0.96; −1.06	+0.69; −0.49	+0.49; −0.42	+0.45; −0.44	+1.82; −0.43	+1.50; −0.88

[a] All data collected with graphite monochromated Mo Kα radiation (λ = 0.710 93 Å) using ω scans. [b] Reflections used to determine the unit cell parameters and their esd's. [c] The unweighted and weighted agreement factors in the least-squares refinements were $R = \sum||F_o| - |F_c||/\sum|F_o|$; $R_w = [(\sum_w(|F_o| - |F_c|)^2/\sum_w F_o^2)]^{1/2}$ where $w = 4F_o^2/s^2(F_o^2)$; $s^2(F_o^2) = [S^2(C + R^2B) + (pF_o^2)^2]/(Lp)^2$, S = scan rate, C = total integrated peak count, R = ratio of scan time to background counting time, B = total background count, Lp = Lorentz-polarization factor, p = p-factor. [d] Maximum negative and positive difference peaks.

Table 2. Selected Bond Lengths in Complexes **1**−**6**[a] (Å)

	1(A)[b]	**1(B)**[b]	**2**	**3**	**4**	**5**	**6**
M−Cl	2.360(2)	2.353(2)	2.318(2)	2.334(1)	2.339(2)	2.245(2)	2.311(3)
M−N_1	2.255(5)	2.277(5)	2.192(6)	2.131(4)	2.072(5)	2.016(6)	2.159(8)
M−N_2	2.212(5)	2.225(5)	2.172(6)	2.120(4)	2.075(5)	2.000(6)	2.191(9)
M−N_5	2.271(5)	2.239(5)	2.192(5)	2.161(4)	2.111(5)		2.145(8)
M−N_3	2.311(4)	2.313(4)	2.281(5)	2.255(4)	2.210(5)	2.298(8)	2.255(8)
M−N_4	2.300(5)	2.302(5)	2.230(6)	2.197(4)	2.152(5)	2.040(7)	2.265(8)

[a] Estimated standard deviations in the least significant figure are given in parentheses. [b] Two independent cations in the asymmetric unit.

ment ranges from 0.312 Å in **1** to 0.125 Å in **4** (Table 4). In **1**−**4**, minor displacements of N_{2-5} from Pl_{eq} occur in an up−down−up−down fashion ($N_2-N_3-N_4-N_5$, respectively).

The cation structure of **5** differs from all others in this paper as the Cu(II) ion adopts a square pyramidal coordination geometry (Figure 4). Four nitrogen donors from PY5 and an exogenous chloride anion compose the coordination sphere. One of the terminal pyridine rings, Py_5, pivots away from the metal center. The coordination geometry is only slightly distorted from an idealized square-pyramidal geometry as compared to a trigonal-bipyramidal geometry as indicated by the distortion parameter $\tau = 0.07$.[20] The equatorial ligands are nitrogens from two terminal pyridines, the nitrogen from the axial pyridine, and the chloride anion (N_2, N_4, N_1, Cl, respectively). The apical position is occupied by the nitrogen from a third terminal pyridine (N_3). The bond lengths of the Cu−N bonds in the equatorial plane are within

Table 3. Selected Angles in **1**−**6**[a] (deg)

	1(A)[b]	**1(B)**[b]	**2**	**3**	**4**	**5**	**6**
Cl_1-M-N_1	176.1(1)	179.1(1)	178.2(2)	178.9(1)	178.0(1)	173.5(2)	178.7(2)
N_1-M-N_2	81.6(2)	79.0(2)	81.9(2)	84.6(1)	87.1(2)	86.5(2)	82.7(3)
N_1-M-N_3	83.1(2)	83.6(2)	83.3(2)	85.3(1)	86.1(2)	86.8(3)	84.6(3)
N_1-M-N_4	83.7(2)	84.7(2)	84.3(2)	86.0(1)	86.8(2)	88.3(2)	86.0(3)
N_1-M-N_5	79.8(2)	80.6(2)	81.6(2)	84.0(1)	86.5(2)		83.9(3)
N_2-M-N_3	79.2(2)	79.0(2)	80.5(2)	81.2(1)	81.6(2)	85.3(3)	81.6(3)
N_2-M-N_5	94.4(2)	92.8(2)	94.3(2)	96.0(1)	96.3(2)		96.1(3)
N_3-M-N_4	100.0(2)	104.6(2)	100.7(2)	100.0(1)	98.9(2)	103.7(3)	99.8(3)
N_4-M-N_5	82.1(2)	79.1(2)	80.9(2)	81.1(1)	82.4(2)		80.2(3)
Py_1-Pl_{eq}[c]	60.9	56.9	61.0	60.9	62.0		64.9

[a] Estimated standard deviations in the least significant figure are given in parentheses. [b] Two independent cations in the asymmetric unit. [c] Intersection of the least-squares pyridine plane Py_1 with the least-squares plane of N_{2-5}, Pl_{eq}.

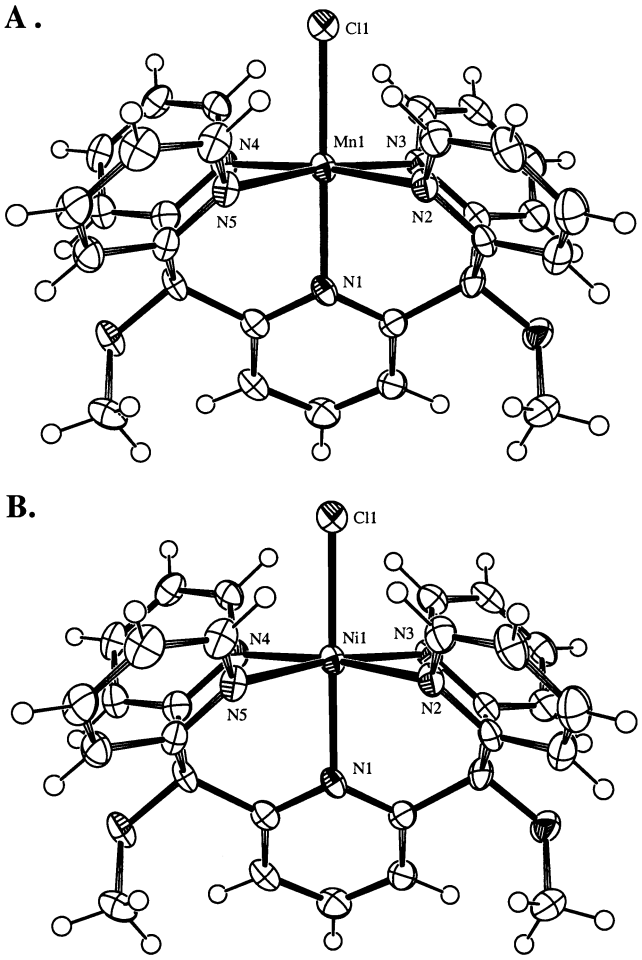

Figure 2. ORTEP representations of the cations of (A) **1**, $[Mn(PY5)(Cl)]^+$, and (B) **4**, $[Ni(PY5)(Cl)]^+$ (50% probability thermal ellipsoids).

the expected range 1.98−2.08 Å for a five-coordinate Cu(II) complex.[21] The bond length between the metal and the apical pyridine is clearly elongated (Cu−N_3, 2.298 Å), consistent with a Jahn−Teller distortion. The 0.137 Å displacement of the Cu(II) ion from the equatorial plane partially accounts for the observed distortion from a square-pyramidal geometry.

Magnetic Properties. The solution magnetic susceptibilities of **1**−**5** (Table 5), as determined by the Evans method,[22] gave magnetic moments near the spin-only values for high-spin (hs) M(II) ions for **1**−**4**. The hs assignments are consistent with the metal ligand distances in the structures (vide supra). No significant changes in magnetic susceptibility are observed for **1**−**4** in the 200−290 K range. For **1**, which contains two hs $[Mn(PY5)(Cl)]^+$ cations for each hs $[MnCl_4]^{2-}$ counteranion, the calculated effective magnetic moment of 5.4 μ_B is the average of the three metal ions. The 4.2 μ_B moment observed for the Co(II) complex, **3**, is consistent with the predicted hs value for an octahedral d^7 complex, with considerable orbital contribution to the overall magnetic moment.[23] For the Ni(II) complex, **4**, the observed

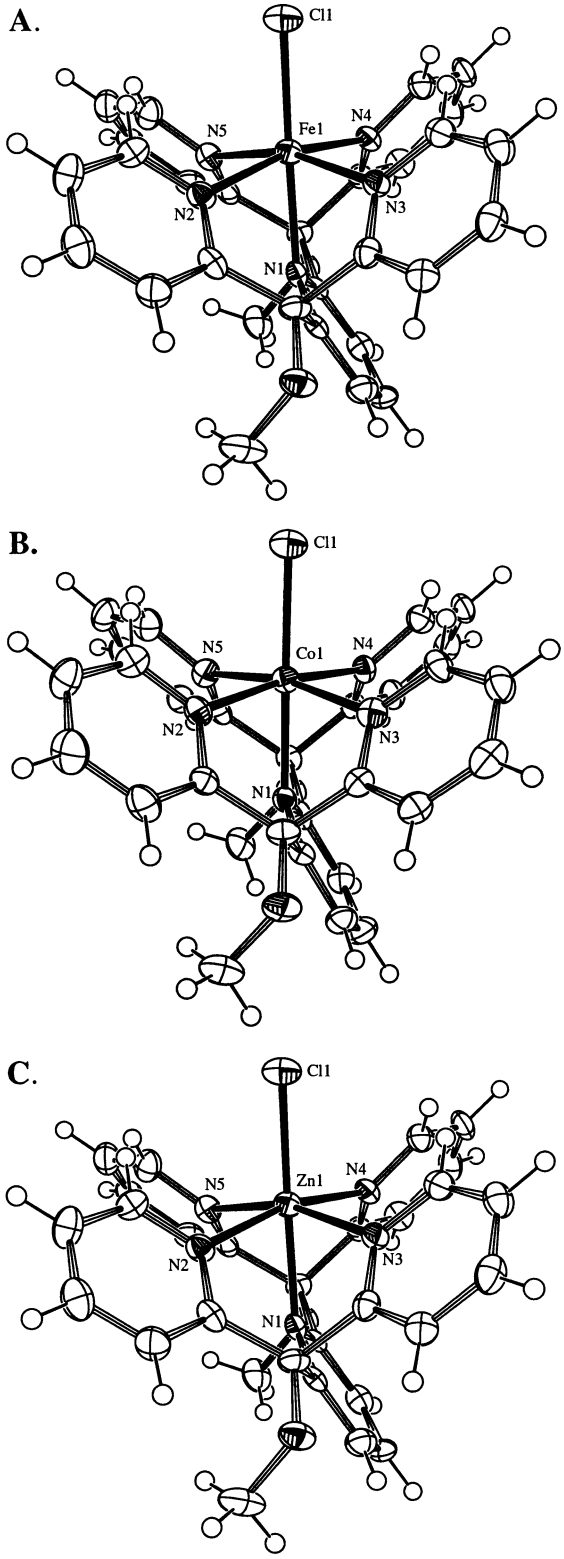

Figure 3. ORTEP representations of the cations of (A) **2**, $[Fe(PY5)(Cl)]^+$, (B) **3**, $[Co(PY5)(Cl)]^+$, and (C) **6**, $[Zn(PY5)(Cl)]^+$ (50% probability thermal ellipsoids). Note the relative invariance in the tilt of Py_1.

effective moment of 2.3 μ_B is low for an octahedral hs complex. Compounds **2** and **4** are both EPR-silent at 77 K, as anticipated for distorted six-coordinate hs Fe(II) and Ni(II)

(20) Addison, A. W.; Rao, T. W.; Reedijk, J.; van Rijn, J.; Verschoor, G. C. *J. Chem. Soc., Dalton Trans.* **1984**, 1349−1356.
(21) Shannon, R. D. *Acta Crystallogr.* **1976**, *A32*, 751−767.
(22) Evans, D. F. *J. Chem. Soc.* **1959**, 2003−2005.
(23) Cotton, F. A.; Wilkinson, G. *Advanced Inorganic Chemistry*, 5th ed.; Wiley-Interscience: New York, 1988.

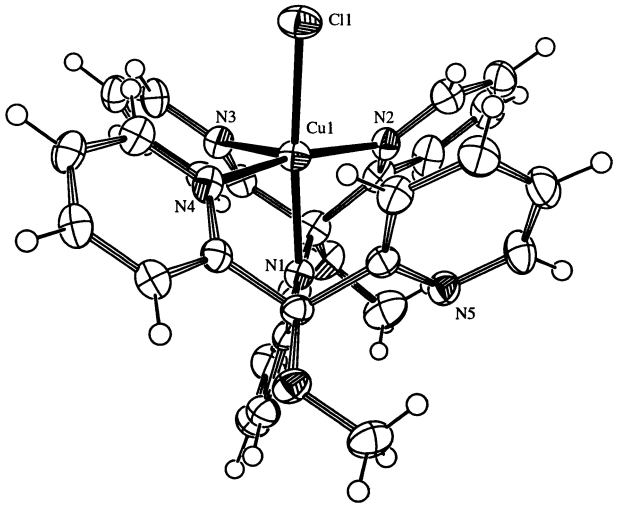

Figure 4. ORTEP representation of the cation of **5**, $[Cu(PY5)(Cl)]^+$, (50% probability thermal ellipsoids) for all non-hydrogen atoms.

Table 4. Equatorial Plane[a] (Pl_{eq}) Deviations in **1**−**6**[b] (Å)

	1(A)[c]	**1(B)**[c]	**2**	**3**	**4**	**5**	**6**
metal ion	0.312	0.311	0.279	0.191	0.125	0.137	0.219
N_1						0.029	
N_2	0.026	−0.005	0.016	0.016	0.014	−0.032	0.0003
N_3	−0.025	0.004	−0.013	−0.014	−0.013		−0.0003
N_4	0.023	−0.004	0.014	0.014	0.014	−0.032	0.0002
N_5	−0.027	0.005	−0.015	−0.016	−0.015		−0.0002
Cl						0.003	

[a] The equatorial plane is defined as the least-squares plane of N_{2-5}, for all complexes except **5** in which N_1, N_2, N_4, and Cl are used. [b] Positive displacements are toward Cl for all structures except **5** where positive displacements are toward N_3. [c] Two independent cations in the asymmetric unit.

complexes with integer spins of $S = 2$ and $S = 1$, respectively. For the Cu(II) complex, **5**, the observed 1.0 μ_B magnetic moment is significantly lower than the idealized spin-only moment. The cause of this reduced moment is currently unknown, though dimer formation in solution is possible. The EPR spectrum of **5** in MeOH at 77 K is axial with $g_\perp = 2.05$ ($A_\perp = 17$ G) and $g_\parallel = 2.23$ ($A_\parallel = 179$ G), fully consistent with the solid-state structure.

UV−Vis Spectroscopy. UV−vis spectra of all complexes in MeOH show strong ligand-based absorptions at ∼250 nm

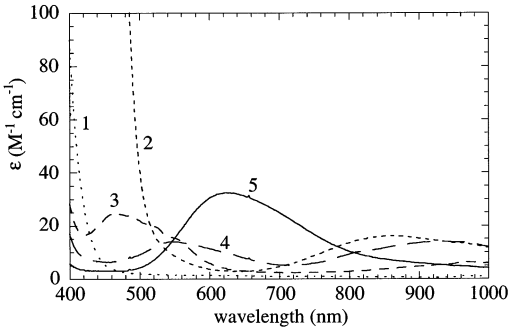

Figure 5. UV−vis spectra (400−1000 nm) of complexes **1**−**5** (∼1.5 mM) in MeOH.

(Table 5). These are the only significant absorption features for **1** and **6**, but complexes **2**−**5** exhibit additional features at lower energy (Figure 5). The Fe(II) complex, **2**, displays an intense absorption at 389 nm ($\epsilon = 1700$ M^{-1} cm^{-1}), assigned as a metal-to-ligand charge transfer (MLCT) band. A single d→d transition is observed at 858 nm without any clear splitting. The Co(II) complex, **3**, shows a multifeatured band of low intensity near 500 nm in addition to an absorption at 970 nm. The anticipated highest energy d→d transition for a distorted-octahedral Co(II) complex is likely obscured by the MLCT bands. For the Ni(II) complex, **4**, two clearly resolved absorptions are observed at 943 and 545 nm. As with **3**, the anticipated highest energy d→d band of **4** is likely obscured by the MLCT bands. For the Cu(II) complex, **5**, a broad d→d transition is observed at 623 nm. These absorption properties in combination with the magnetic moments are consistent with the solid-state structural characterization of complexes **1**−**4** as hs distorted-octahedral complexes and confirm the structural integrity of the complexes dissolved in MeOH.

Electrochemical Properties. Cyclic voltammetric examination of **1**−**6** in MeCN under N_2 shows a number of oxidative and reductive features (Table 5). The ligand oxidation and reduction potentials are greater than +1.0 V and less than −2.3 V versus Fc/Fc^+, respectively, as **6** is redox inactive in this range. Complexes **1**, **2**, and **4** exhibit a single oxidative response, likely associated with the M^{2+}/M^{3+} transition. The Co(II) complex **3** displays two consecu-

Table 5. Selected Physical Properties of **1**−**6**

1	**2**	**3**	**4**	**5**	**6**
		298 K μ_{eff}[a] (μ_B)			
9.4 (5.5 per metal)	4.7	4.2	2.3	1.0	
		200 K μ_{eff}[a] (μ_B)			
9.4 (5.4 per metal)	4.6	4.3	2.5		
		UV−Vis[b] (nm)			
246 (12 100)	249 (8400)	262 (15 800)	249 (8700)	250 (12 900)	250 (19 300)
330 (sh, 740)	320 (1600)	463 (25)	305 (sh, 730)	623 (80)	
	390 (1690)	522 (20)	545 (14)		
	858 (16)	549 (15)	934 (14)		
		969 (7)			
		CV[c] (V)			
0.66 (rev)	0.40 (rev)	0.51 (irrev)	0.39 (rev)	−0.56 (rev)	
−2.22 (irrev)	−2.07 (irrev)	0.15 (rev)	−1.91 (irrev)	−1.12 (irrev)	
		−1.70 (irrev)	−2.40 (irrev)		

[a] Average of two independent determinations given in μ_B. 200 K measurements are corrected for solvent contraction. [b] Extinction coefficients are given in parentheses after each feature. [c] Potentials reported in V vs Fc/Fc^+.

tive oxidations at 0.15 and 0.51 V; the first is reversible while the second feature is not. On the basis of their reversibilities, these features likely correspond to Co(II)/Co(III) and Co(III)/Co(IV) processes, respectively. No oxidative features are observed for Cu(II) complex **5**.

Complexes **1**−**3** show a single irreversible reductive feature at approximately −2.0 V. The absence of this feature for the Zn(II) complex suggests that these features are metal-based and not ligand-based reductions. The Ni(II) complex, **4**, is reduced via two consecutive irreversible steps at −1.9 and −2.4 V. Two reductions are observed for complex **5** at −0.56 and −1.1 V. The first quasireversible reduction likely derives from a Cu(II)/Cu(I) process.

Discussion

Structural examination of a series of first-row transition metal complexes derived from the pentadentate ligand PY5 and chloride illustrates the ability of this ligand to accommodate a variety of divalent metal ions. While the Cu(II) complex (**5**) contains a five-coordinate metal ion in a distorted square-pyramidal geometry, the Mn(II), Fe(II), Co(II), Ni(II), and Zn(II) complexes (**1**−**4**, and **6**, respectively) all contain a six-coordinate metal ion in a slightly distorted octahedral geometry. This isostructural series evinces general trends in the coordination properties of the PY5 ligand.

Deviations from an ideal octahedral geometry in **1**−**4** and **6** are evident from the various bond angles between the central metal ion and its equatorial nitrogen ligands, N_{2-5} (Table 3). The N−M−N angles between N_2 and N_3 and between N_4 and N_5 are distinctly smaller than the ideal 90°; values range from 79.0° to 82.4°. Consequently, the bond angles between N_2 and N_5 and between N_3 and N_4 are larger than 90°. Only minor distortions are found along the axial axis; all N_1−M−Cl bond angles deviate <4° from linearity.

More significant deviations from an ideal octahedral geometry derive from the lengths of the M−N bonds. In **1**−**4** and **6**, M−N_2 and M−N_5 are consistently shorter than M−N_3 and M−N_4 (Table 2), a trend previously noted in [Fe^{III}(PY5)(OMe)](OTf)$_2$[17,18] and a series of [Fe(II)(PY5)(X)] complexes.[19] These systematic variations in the equatorial M−N distances are associated with the distinctive tilt of the axial pyridine Py_1 and correlated arrangement of the methoxy groups of the ligand. To facilitate structural comparisons, an equatorial plane (Pl_{eq}) is conveniently defined by the least-squares plane of the four terminal pyridine nitrogen atoms, N_{2-5}, while the axial positions are occupied by the axial pyridine nitrogen N_1 and an exogenous chloride anion. The conformations of the free ligand structure[18] and of the metal complexes are very different. In the free ligand, the plane of Py_1 is perpendicular to Pl_{eq}, and the methyls of the methoxy groups are positioned away from Py_1 into the two clefts defined by Py_2/Py_3 and Py_4/Py_5 (Figure 1). Upon binding a metal, Py_1 tilts to 65−57° relative to Pl_{eq} (a 25−33° tilt relative to perpendicular, Table 3) for **1**−**6**, and the two methoxy groups are positioned into different clefts defined by Py_2/Py_1 and Py_1/Py_5. The nearly invariant tilts of Py_1 from Mn (d^5) to Zn (d^{10}) suggest that any metal−Py_1 π-bonding interactions cannot be a significant contributor to the stabilization of this distinctive ligand conformation.

Although the arrangement of the methoxy groups might seem of minor importance, their positioning is structurally noninnocent as previously noted in a related set of ligands.[18,24] Structures of triarylmethyl methyl ethers show that the cleft angles, the angles at the four-coordinate carbon connecting the pyridyl rings, significantly deviate from the ideal 109° angle; positioning the ether group into one cleft significantly increases that specific cleft angle while decreasing the remaining two.[18,24] The tilt of Py_1 is readily associated with the increased cleft angle as seen in Figure 3. Also note the correlated arrangement of the methoxy group. This methoxy group positioning and the tilt of Py_1 combine to structurally differentiate the four terminal pyridines into two groups, Py_2/Py_5 and Py_3/Py_4. The former group of pyridine subunits binds more tightly to the metal center than the latter (Table 2, Figure 1). A clear understanding of this trend is currently unknown and will require more extensive electronic calculations.

What is clear from the structures is that this distinctive conformation of the ligand yields five M−N distances in the ∼2.2 Å range, a distance appropriate for a divalent, first-row transition metal. One might anticipate that such a coordination environment could be achieved by maintaining a more symmetric conformation as observed in the free ligand structure. Only one metal complex is currently known that adopts this ligand conformation, [Cu^{II}(PY5)(OTf)](OTf) (OTf = $CF_3SO_3^-$, triflate anion).[25] The Cu(II) ion in this structure is six-coordinate, similar to **1**−**4** and **6** except that a triflate anion replaces the axial chloride.[25] The methoxy groups are positioned in the Py_2/Py_3 and Py_4/Py_5 clefts similar to the free ligand structure. A significant and understandable difference in this structure is the inequivalence of the 5 Cu−N distances; the four equatorial distances average ∼2.0 Å while the Cu−N_1 distance of Py_1 along the Jahn−Teller axis is ∼2.3 Å. Apparently, the energetic cost of creating five equivalent M−N distances in the ∼2.2 Å range is reduced if the ligand adopts a less symmetric conformation.

A closer comparison between the complexes was obtained by overlaying the three-dimensional structures of the cations, using the cation of the Ni(II) complex, **4**, as a reference. The cations of complexes **1**−**4** and **6** are indeed isostructural, as RMS values of only 0.125 Å for **1**, 0.083 Å for **2**, 0.046 Å for **3**, and 0.080 Å for **6** are calculated. In each case, the largest single contribution to these RMS deviation values comes from the displacement of M(II) from Pl_{eq}.

A large deviation from an ideal octahedral geometry derives from the displacement of the metal ion from Pl_{eq} toward the chloride anion. The extremes in this displacement are the Ni(II) complex, **4** (0.125 Å), the metal coordination of which seems closest to an ideal octahedron, and the Mn(II) complex, **1** (0.312 Å) (Figure 6). Proceeding from Mn(II) to Zn(II) in a six-coordinate, high-spin (hs) electron configuration, the ionic radius of the metal ion decreases from 0.97

(24) Jonas, R. T.; Stack, T. D. P. *Inorg. Chem.* **1998**, *37*, 6615−6629.
(25) Unpublished results.

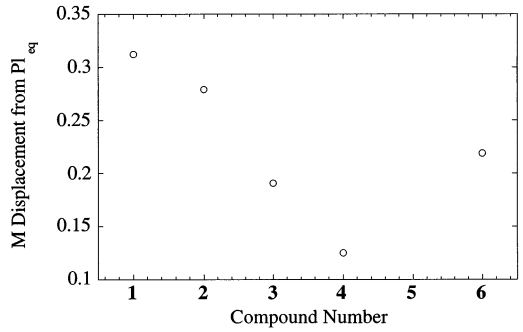

Figure 6. Plot of metal(II) displacement from equatorial plane Pl_{eq} for octahedral compounds **1**−**4** and **6**.

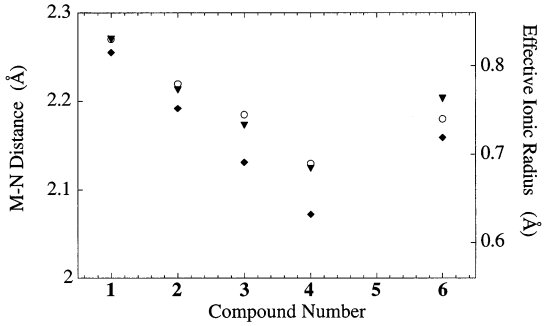

Figure 7. Plot of M−N distances in **1**−**4** and **6** and effective ionic radius (○) for six-coordinate metals.[21] $M-N_1$ distance (◆), and the average $M-N_{2-5}$ distance (▼).

Å for Mn(II) to 0.63 Å for Ni(II) and increases again to 0.88 Å for Zn(II) (Figure 7).[21] This trend coincides directly with the metal displacement from Pl_{eq} in these PY5 complexes and suggests that the pocket created by the ligand is actually somewhat small to accommodate a divalent first-row transition metal ion.

Within the present series of $[M^{II}(PY5)(Cl)]^+$ complexes, the structure of the Cu(II) complex is distinctly different from the other complexes. Whereas all complexes contain a six-coordinate metal ion in a distorted-octahedral geometry, **5** contains a five-coordinate metal ion in a square-pyramidal geometry. This observation seems remarkable within the PY5 series but is not surprising when compared with other Cu(II) complexes. A search in the Cambridge Structural Database for copper complexes with a N_5Cl ligand set yields only two examples.[26,27] In contrast, numerous examples of Cu(II) complexes are known with a N_4Cl ligand set, similar to the cation geometry found in complex **5**. A striking feature of the structure of **5** is the almost perfect square-pyramidal geometry around Cu(II) ($\tau = 0.07$). This is accomplished by a simple rotation of Py_5 that orients the metal ion 2.8 Å above the least-squares plane of the pyridine subunit. The potential coordination site is left vacant in complex **5** (Figure 4); this vacancy likely results from the enhanced metrical demands along this Jahn−Teller axis. Py_5 does coordinate to Cu(II) upon displacement of the chloride ions for weakly coordinating triflate ions, as found for the aforementioned [Cu(PY5)(OTf)](OTf).[25] Apart from the noncoordinating terminal pyridine Py_5, **5** is structurally related to the other PY5 complexes. A comparison of its cation coordination geometry with that of Ni(II) complex **4** shows that the cations deviate only by a RMS of 0.128 Å when the Py_5 rings of both complexes are excluded from the analysis. This can be interpreted as a strong preference of the PY5 ligand to bind metal ions at five apices of an octahedron, a principal design feature of the PY5 ligand.

The PY5 ligand provides the metals in complexes **1**−**6** with a nitrogen-rich, neutral, six-coordinate ligand field. The d→d band patterns measured in MeOH are consistent with a distorted octahedral coordination; the two transitions observed for Ni(II) complex **4** are similar both in energy and intensity to the d→d bands seen for $[Ni(pyridine)_6]^{2+}$. On the basis of the presence of five pyridine rings, the PY5 ligand could be considered as a strong-field ligand within the spectrochemical series, giving rise to metal complexes with low-spin (ls) electron configurations. However, all PY5 complexes discussed in this paper behave as hs complexes in the range 200−300 K. Apparently, the weak-field character of the chloride overrides the strong-field tendencies of the pyridine ligands. Recent studies in this laboratory have shown that the room-temperature electron configuration of the PY5 metal complexes is sensitive to changes in ligation at the sixth, axial position.[19]

In the octahedral complexes, the metal ions are stabilized in a metal(II) oxidation state by the neutrally charged, aromatic amine donors; for example, no oxidation in air is observed for the Fe(II) complex, **2**. Oxidation to the M(III) level occurs between 0.15 and 0.66 V versus Fc/Fc^+, whereas reduction to lower oxidation states occurs between −1.70 and −2.22 V. The M(II) state thus covers a range 1.85−2.88 V in the PY5 complexes. These values show the strong tendency of the PY5 ligand to complex transition metal ions in a divalent oxidation state.

Concluding Remarks

The structural analysis of a series of transition metal complexes derived from the pentadentate ligand PY5 demonstrates the intrinsic property of this ligand to complex divalent metal ions in a six-coordinate fashion. Electronic preferences (that is, Jahn−Teller effects) can override this proclivity if a strong exogenous ligand, such as Cl^-, is available. The fact that this ligand can adapt itself to various metal ion sizes makes it a versatile building block for the construction of new octahedral metal complexes and for the study of biologically relevant six-coordinate complexes. The structural trends outlined in this paper will serve as a guideline in these studies. A complementary study focuses on the control of the spin-state in these complexes via variation of the axial ligand and on the substitution behavior of the labile axial ligand.

Experimental Section

Instrumentation. Electronic spectra at room temperature (RT) were measured on a Hewlett-Packard 8435 spectrophotometer. Electrochemical measurements were recorded in acetonitrile (MeCN)

(26) Parker, O. J.; Breneman, G. L. *Acta Crystallogr., Sect. C* **1995**, *51*, 1529−1531.
(27) Ainscough, E. W.; Brodie, A. M.; Depree, C. V. *J. Chem. Soc., Dalton Trans.* **1999**, 4123−4124.

solutions at 100 mV/s in a drybox at RT using a BAS CV-50W voltammetric analyzer, a platinum working electrode, a platinum wire auxiliary electrode, 0.1 M (n-Bu_4N)(ClO_4) supporting electrolyte, and a Ag/AgCl wire reference electrode. All potentials were referenced to Fc/Fc^+. ^1H NMR spectra were recorded on a Varian Gemini-400 NMR spectrometer at RT; solution magnetic moments were determined in CD_3OD at RT and 200 K by Evans' method.[22] EPR spectra were recorded on a Bruker ER 220 D-SRC at 77 K. Mass spectrometry data were collected by the Mass Spectrometry Facility, Department of Pharmaceutical Chemistry, University of California, San Francisco. Elemental analyses were performed by Midwest Microlabs (Indianapolis, IN) and Desert Analytics (Tucson, AZ); samples were dried under vacuum overnight prior to analysis and handled aerobically.

Syntheses. Chemicals were purchased from Aldrich Chemicals and used without further purification unless noted otherwise. Methanol (MeOH) was distilled over $Mg(OMe)_2$ prior to use. 2,6-(Bis-(bis-2-pyridyl)methoxymethane)pyridine, PY5, was synthesized according to a procedure reported earlier.[17]

[Mn(PY5)(Cl)]$_2$(MnCl$_4$) (1). A MeOH solution (20 mL) containing PY5 (194 mg, 0.41 mmol) and $MnCl_2 \cdot 4H_2O$ (121 mg, 0.61 mmol) was refluxed under N_2 for 30 min. The resulting pale yellow solution was passed through a glass filter while still hot, and the filtrate was concentrated in vacuo. Layering with Et_2O induced crystallization. Yield: 235 mg (~80%) of **1** as pale yellow crystals. Single crystals suitable for X-ray analysis were obtained by vapor diffusion of diethyl ether (Et_2O) into a concentrated MeOH solution. Absorption spectrum (MeOH): λ_{max} (nm), ϵ (M^{-1} cm^{-1}): 246, 12 100; 330 (sh), 750. Mass spectrometry ($LSIMS^+$): m/e 565.0 (**1**$^+$). Cyclic voltammetry (MeCN vs Fc/Fc^+): 0.66 V (ΔE = 70 mV, i_{pa}/i_{pc} = 1); −2.22 V (irreversible). Solution magnetic moment (CD_3OD): μ_{eff} = 9.4 μ_B. Anal. Calcd for $C_{58}H_{50}O_4N_{10}Cl_6Mn_3$: C, 51.75; H, 4.20; N, 10.06. Found: C, 51.54; H, 4.08; N, 10.13.

[Fe(PY5)(Cl)](Cl) (2). Equimolar amounts of anhydrous $FeCl_2$ (56 mg, 0.44 mmol) and PY5 (210 mg, 0.44 mmol) were combined in MeOH (50 mL). The resulting mixture was refluxed under N_2 for 2.5 h. The hot, bright yellow solution was passed through a glass filter, and the filtrate was concentrated in vacuo. Layering with Et_2O induced crystallization. Yield: 175 mg (~60%) of **2** as yellow crystals. Single crystals suitable for X-ray analysis were obtained by vapor diffusion of Et_2O into a concentrated MeOH solution. Absorption spectrum (MeOH): λ_{max} (nm), ϵ (M^{-1} cm^{-1}): 249, 8400; 320, 1600; 389, 1700; 858, 15. Cyclic voltammetry (MeCN vs Fc/Fc^+): 0.40 V (ΔE = 80 mV, i_{pa}/i_{pc} = 0.9); −2.07 V (irreversible). Solution magnetic moment (CD_3OD): μ_{eff} = 4.7 μ_B. Anal. Calcd for $C_{29}H_{25}O_2N_5Cl_2Fe \cdot MeOH$: C, 54.91; H, 4.61; N, 11.04. Found: C, 55.08; H, 4.63; N, 11.00.

[Co(PY5)(Cl)](Cl) (3). Equimolar amounts of PY5 (208 mg, 0.44 mmol) and $CoCl_2$ (57 mg, 0.44 mmol) were combined in MeOH (50 mL). The resulting mixture was refluxed under N_2 for 2.5 h. The hot, pink solution was passed through a glass filter, and the filtrate was concentrated in vacuo. Layering with Et_2O induced crystallization. Yield: 195 mg (~65%) of **3** as pink crystals. Single crystals suitable for X-ray analysis were obtained by vapor diffusion of Et_2O into a concentrated MeOH solution. Absorption spectrum (MeOH): λ_{max} (nm), ϵ (M^{-1} cm^{-1}): 262, 15 800; 463, 25; 522, 20; 549, 15; 969, 7. Mass spectrometry ($LSIMS^+$): m/e 569.0 (**3**$^+$). Cyclic voltammetry (MeCN vs Fc/Fc^+): 0.51 V (ΔE = 80 mV, i_{pa}/i_{pc} = 1); 0.15 (ΔE = 190 mV, i_{pa}/i_{pc} = 0.36); −1.70 V (irreversible). Solution magnetic moment (CD_3OD): μ_{eff} = 4.2 μ_B. Anal. Calcd for $C_{29}H_{25}O_2N_5Cl_2Co \cdot 2H_2O$: C, 54.30; H, 4.56; N, 10.92. Found: C, 54.16; H, 4.57; N, 10.92.

[Ni(PY5)(Cl)](Cl) (4). Equimolar amounts of PY5 (196 mg, 0.41 mmol) and $NiCl_2 \cdot 4H_2O$ (98 mg, 0.41 mmol) were combined in MeOH (50 mL). The resulting mixture was refluxed under N_2 for 2.5 h. The hot, purple solution was passed through a glass filter, and the filtrate was concentrated in vacuo. Layering with Et_2O induced crystallization. Yield: 175 mg (~65%) of **4** as purple crystals. Single crystals suitable for X-ray analysis were obtained by vapor diffusion of Et_2O into a concentrated MeOH solution. Absorption spectrum (MeOH): λ_{max} (nm), ϵ (M^{-1} cm^{-1}): 249, 8700; 305 (sh), 750; 545, 14; 934, 14. Mass spectrometry ($LSIMS^+$): m/e 568.0 (**4**$^+$). Cyclic voltammetry (MeCN vs Fc/Fc^+): 0.39 V (ΔE = 290 mV, i_{pa}/i_{pc} = 0.71); −1.91, −2.40 V (irreversible). Solution magnetic moment (CD_3OD): μ_{eff} = 2.3 μ_B. Anal. Calcd for $C_{29}H_{25}O_2N_5Cl_2Ni \cdot 4H_2O$: C, 51.43; H, 4.91; N, 10.34. Found: C, 51.43; H, 4.31; N, 10.31.

[Cu(PY5)(Cl)](Cl) (5). Equimolar amounts of PY5 (205 mg, 0.43 mmol) and $CuCl_2 \cdot 2H_2O$ (57 mg, 0.44 mmol) were dissolved in MeOH (50 mL). The resulting mixture was refluxed under N_2 for 2.5 h. The hot, blue solution was passed through a glass filter, and the filtrate was concentrated in vacuo. Yield: 285 mg (~95%) of **5** as a greenish blue powder. Single crystals suitable for X-ray analysis were obtained by vapor diffusion of Et_2O into a concentrated MeOH solution. Absorption spectrum (MeOH): λ_{max} (nm), ϵ (M^{-1} cm^{-1}): 250, 12 900; 623, 35. Cyclic voltammetry (MeCN vs Fc/Fc^+): −0.56 V (ΔE = 60 mV, i_{pa}/i_{pc} = 0.6); −1.12 V (irreversible). Solution magnetic moment (CD_3OD): μ_{eff} = 1.0 μ_B. Anal. Calcd for $C_{29}H_{25}O_2N_5Cl_2Cu \cdot 1.5MeOH$: C, 52.93; H, 4.75; N, 10.65. Found: C, 53.18; H, 4.62; N, 10.76.

[Zn(PY5)(Cl)]$_2$(ZnCl$_4$) (6). A solution of PY5 (228 mg, 0.48 mmol) in MeOH (10 mL) was combined with anhydrous $ZnCl_2$ (98 mg, 0.72 mmol) dissolved in 10 mL of MeOH, which resulted in a white precipitate. Refluxing the reaction mixture under N_2 for 30 min resulted in a clear, yellowish solution. After removal of the solvent in vacuo, the residue was washed with CH_2Cl_2 until colorless. Recrystallization from a $MeCN/H_2O/Et_2O$ solution gave 45 mg (~10%) of **6** as a white powder. Single crystals suitable for X-ray analysis were obtained by vapor diffusion of Et_2O into a concentrated $MeCN/H_2O$ solution. Absorption spectrum (MeOH): λ_{max} (nm), ϵ (M^{-1} cm^{-1}): 250, 19 300. ^1H NMR (CD_3CN/D_2O, 400 MHz): δ 3.68 (s, 6H, OCH_3), 7.53 (m, 4H, PyH), 7.96 (m, 8H, PyH), 9.28 (m, 4H, PyH). An acceptable elemental analysis could not be obtained. The related complex [Zn(PY5)(Cl)](OTf) was made in higher yield and purity. Anhydrous $Zn(OTf)_2$ (53 mg, 0.146 mmol) was combined with PY5 (67 mg, 0.14 mmol) and dissolved in 2.0 mL of MeOH. Addition of Et_4NCl (23 mg, 0.14 mmol) in 0.4 mL of MeOH caused a white solid to precipitate. This solid was washed with diethyl ether and dried. Yield: 69 mg (~65%). The ^1H NMR was identical to that of **6**, suggesting that the same cation was formed. Anal. Calcd for $C_{30}H_{25}O_5N_5ClF_3SZn$: C, 49.67; H, 3.47; N, 9.66. Found: C, 49.34; H, 3.39; N, 9.33.

X-ray Structure Analysis. The structure analyses of single crystals obtained from compounds **1**−**6** were all performed using the procedures outlined in the following paragraphs.

Data Collection. Crystals of **1**−**6** were mounted on a glass fiber with paratone oil and placed on a Enraf-Nonius CAD-4 diffractometer (**1**−**4**) or a Siemens SMART diffractometer (**5**−**6**) under a cold stream of N_2. All measurements were made with graphite monochromated Mo Kα radiation (λ = 0.710 93 Å). Cell constants and an orientation matrix for data collection were obtained from a least-squares refinement using setting angles of typically 25 carefully centered reflections (CAD-4) or >4000 (SMART). The data were collected at reduced temperatures using the ω scan

technique to a maximum 2θ value of 50° for **1**−**4** and 52.2° for **5** and **6**. A summary of the crystal data and data collection details is presented in Table 1.

Data reduction for complexes **1**−**4** was performed as follows. The intensities of three representative reflections were measured after every 60 min, and two orientational reflections were measured every 200 reflections. Over the course of data collection, the standards generally decreased. An appropriate linear correction factor was applied to all data sets (**1**−**4**) to account for this phenomenon. An empirical absorption correction was applied, if deemed necessary, on the basis of azimuthal scans of several reflections. The data were corrected for Lorentz and polarization effects. In the case of complexes **5** and **6**, data were integrated using the program SAINT v. 4.024 (Siemens Industrial Automation, Inc.) with a 1.6° × 1.6° × 0.6° box. No decay correction was necessary for these two data sets. An empirical absorption correction, XPREP, was applied, and the data were further corrected for Lorentz and polarization effects.

All the structures were solved by direct methods and expanded using Fourier techniques. All non-hydrogen atoms were refined anisotropically. Hydrogen atoms were placed at idealized positions 0.95 Å from their parent atoms before the final cycle of refinement. All calculations were performed using the teXsan crystallographic software package of Molecular Structure Corporation.

Acknowledgment. We are grateful to the National Institutes of Health (Grant GM50730), the Netherlands Organization for Scientific Research (R.J.M.K.G.), and the Stanford Graduate Fellowship Fund (C.R.G.) for financial support of this work. Mass spectra were performed by the Mass Spectrometry Facility, Department of Pharmaceutical Chemistry, University of California, San Francisco.

Supporting Information Available: ORTEP representations and complete tables of positional parameters, bond lengths, bond angles, and anisotropic thermal factors for all structures. This material is available free of charge via the Internet at http://pubs.acs.org.

IC025617R